

## Article

# Mesoporous VCN Nanobelts for High-Performance Flexible Zn-Ion Batteries

Zeyan Zhou <sup>1,\*</sup> , Taotao Zeng <sup>1</sup>, Haoran Zhang <sup>2</sup> and Ding Chen <sup>1,3,\*</sup> <sup>1</sup> School of Materials Science and Engineering, Hunan University, Changsha 410082, China; ttzeng@hnu.edu.cn<sup>2</sup> National Engineering Research Center for Marine Aquaculture, Marine Science and Technology College, Zhejiang Ocean University, Zhoushan 316004, China; hr\_zhang99@163.com<sup>3</sup> State Key Laboratory of Advanced Design and Manufacturing for Vehicle Body, College of Mechanical and Vehicle Engineering, Hunan University, Changsha 410082, China

\* Correspondence: zhouzeyan@hnu.edu.cn (Z.Z.); chending@hnu.edu.cn (D.C.)

**Abstract:** Vanadium nitride (VN) with a wide working window has been identified as a promising electrode material candidate for batteries due to the high specific capacitance and the excellent electrical conductivity. Here, we have successfully prepared VCN nanobelts, which display mesoporous structure with high specific surface area ( $54.4 \text{ m}^2 \text{ g}^{-1}$ ) and the total pore volume was  $0.266 \text{ cm}^3 \text{ g}^{-1}$ . Furthermore, the prepared flexible Zn-ion battery (FZIB) with VCN-5 not only exhibited high specific capacitance ( $81 \mu\text{Ah cm}^{-2}$ ), excellent rate capability, and long cyclic durability (77% after 1000 cycles at  $0.6 \text{ mA cm}^{-2}$ ) but also had the characteristics of flexibility. This FZIB is important to reduce the difficulty in thermal management and can be used in a series of applications, including wearable electric devices.

**Keywords:** VCN; energy storage; flexible; Zn-ion batteries

**Citation:** Zhou, Z.; Zeng, T.; Zhang, H.; Chen, D. Mesoporous VCN Nanobelts for High-Performance Flexible Zn-Ion Batteries. *Energies* **2022**, *15*, 4932. <https://doi.org/10.3390/en15134932>

Academic Editors: Qiuwang Wang, Wenxiao Chu, Lizhong Yang and Antonino S. Aricò

Received: 30 May 2022

Accepted: 4 July 2022

Published: 5 July 2022

**Publisher's Note:** MDPI stays neutral with regard to jurisdictional claims in published maps and institutional affiliations.



**Copyright:** © 2022 by the authors. Licensee MDPI, Basel, Switzerland. This article is an open access article distributed under the terms and conditions of the Creative Commons Attribution (CC BY) license (<https://creativecommons.org/licenses/by/4.0/>).

## 1. Introduction

With the remarkable development of low-cost, lightweight, portable electronic devices, electrical vehicles, and aerospace and medical systems in our daily lives, the demand for a sustainable energy supply is becoming one of the greatest challenges for the whole world [1–3]. As we all know, some energy storage devices may also lead to complex thermal management strategies due to high heat generation. As a result, people pay more and more attention to green energy, electrochemical energy storage devices with low resistance, such as advanced energy storage devices, and batteries play a vital role in solving the earth's energy crisis and developing sustainable green energy [4]. Because of its high energy density, long cycle life, and many other advantages, batteries occupy a dominant position in portable electronic products and emerging electric/hybrid vehicles. Lithium-ion batteries (LIBs) are now considered a possible choice for electric vehicles and grid-level energy storage systems in the future. However, there are disadvantages, like high cost and safety issues, which strongly limit their further development for large-scale applications [5]. It is well known that sodium and potassium are not only cheaper than lithium, but also have similar chemical properties to lithium. Therefore, sodium-ion batteries (SIBs) and potassium-ion batteries (KIBs) have great potential to replace lithium-ion batteries and play a role in energy storage in the future. Nevertheless, with more and more in-depth studies of sodium-ion batteries and potassium-ion batteries, their shortcomings, such as low energy density, use of highly toxic and flammable electrolytes, high operating costs, and safety problems, have attracted more and more attention. As a result, researchers have to develop other energy storage alternatives [6–8].

In this regard, zinc-ion batteries (ZIBs) have a special prospect compared with the above-mentioned energy storage devices [9]. In 1799, Volta et al. firstly used metallic zinc (Zn) in the primary battery; Zn anode was considered an excellent negative electrode for

the primary and secondary Zn-based batteries (e.g., Zn-air, Zn-Mn, and Ni-Zn batteries), due to their high theoretic capacities, low potential, high safety, and low cost [10–12].

It is worth noting that compared with the single electron transfer in lithium-ion batteries, zinc-based batteries use double electron transfer in the charge and discharge process, which allows them to provide high mass capacity ( $820 \text{ mAh g}^{-1}$ ) and high volume capacity ( $5855 \text{ mAh cm}^{-3}$ ). On the one hand, the aqueous solution of zinc-ion batteries not only provides faster ion diffusion than non-aqueous electrolyte in lithium-ion batteries, but also ensures the safety of micro-devices. On the other hand, the high redox potential of zinc-based MESD ( $-0.763 \text{ nm V}$  vs. standard hydrogen electrode) enables zinc-ion batteries to work stably in aqueous electrolytes, which is difficult for lithium-ion batteries to achieve. In addition, the reversibility of zinc insertion/extraction in the electrolytes can protect the zinc anode from the formation of zinc dendrites and other byproducts. Considering the above situation, zinc-ion batteries are expected to be very promising in high performance, miniaturization, and integrated wearable electronic products.

Both Mn-based or Mo-based Zn batteries occupy an important position in the battery field because of their high electrochemical performance [13]. Although manganese-based zinc-ion batteries have great development potential, due to the formation of zinc dendrites and irreversible discharge materials in the electrochemical process, the ions in the electrolyte can not migrate better in the active materials and the active materials are oxidized and inactivated, resulting in poor cycle life and poor discharge performance [14–16].

There is no doubt that due to the low cost of vanadium nitride and rich resources, vanadium-based zinc-ion batteries seems to be a potential energy storage device. Most of them show good electrochemical performance in electrochemical work. With the advantages of high specific capacity, excellent rate performance and long cycle life, they play an important role in modern advanced energy storage devices. In the last few years, vanadium nitride (VN) has become a very promising electrochemical active material, which has attracted more and more researchers' attention. It has remarkable electrical conductivity ( $1.67 \times 10^6 \Omega^{-1} \text{ m}^{-1}$ ), as well as high specific surface area and specific capacitance, and a wide 1.2 V voltage window, indicating great potential to realize high electrochemical performance energy storage devices.

In our previous research [17], we demonstrated a porous VN nanomaterial electrode preparation method, which can effectively fabricate uniform pore diameter nanostructures with a specific surface area of  $46.5 \text{ m}^2 \text{ g}^{-1}$  by nitriding etching under  $\text{N}_2/\text{NH}_3$  atmosphere. Such porous electrode material shows excellent electrochemical performance. Unfortunately, its cyclical stability is not excellent. The present work may contribute to the development of energy storage devices with high electrochemical performance. In order to improve the poor cycle stability of VN electrode, the introduction of C element into the preparation of VN may be one of the effective means.

In this work, we have successfully prepared VCN (Vanadium Carbon Nitride) nanobelts, which display mesoporous structure with a high specific surface area ( $54.4 \text{ m}^2 \text{ g}^{-1}$ ) and the total pore volume was  $0.266 \text{ cm}^3 \text{ g}^{-1}$ . Furthermore, the prepared flexible Zn-ion battery (FZIB) with VCN-5 not only exhibited high specific capacitance ( $81 \mu\text{Ah cm}^{-2}$ ), remarkable rate capability, and long periodic stability. (77% after 1000 cycles at  $0.6 \text{ mA cm}^{-2}$ ) but also had the characteristics of flexibility. This FZIB is important for the development of applications such as miniaturized, flexible, portable, and wearable electronics while reducing the difficulty in thermal management.

## 2. Materials and Methods

### 2.1. Materials

Polyvinyl alcohol (PVA) (molecule weight: 44.05) and glucose ( $\text{C}_6\text{H}_{12}\text{O}_6$ ) were obtained from Sigma-Aldrich company (Shanghai, China).  $\text{ZnSO}_4$  and KOH (85%) were bought from Aladdin Company (Shanghai, China). Melamine (AR, 99%) and ammonium metavanadate (AR, 99%) were purchased from Alfa Aesar, Shanghai, China. Zinc sheets (99%) were purchased from Gaoke New Materials Co., Ltd. (Guangzhou, China).

## 2.2. Synthesis of VN and VCN-n

All reactants were analytically pure and used without further purification. Firstly, ammonium metavanadate of 3 mmol and melamine of 40 mmol were dissolved in deionized water of 60 mL and stirred at room temperature for 8 h. Then, the products were collected, filtered, and dried at 70 °C for 48 h. Then, after grinding with mortar, the products powder was put into a glass tube furnace and annealed at 900 °C in N<sub>2</sub> atmosphere for 2 h.

For the fabrication of VCN-n, three different concentrations (3 mmol, 9 mmol, and 15 mmol C<sub>6</sub>H<sub>12</sub>O<sub>6</sub> were named VCN-1, VCN-3, and VCN-5, respectively) of glucose were added to a 3 mmol ammonium metavanadate and 40 mmol melamine blend and stirred vigorously for 6 h followed by ultra-sonication with 60 mL DI water. All further steps for VCN-n fabrication are similar to the steps used for VN.

## 2.3. Synthesis of Zn-PVA Hydrogels

First, a 4 g PVA powder sample was dissolved in 40 mL of distilled water and stirred at 90 °C for 2 h until the solution was clarified. Once the solution clarified, different volumes of KOH 6M were added and stirring was maintained. The resulting liquid was then poured into a covered petri dish and released in a controlled atmosphere to avoid the presence of carbon dioxide. After that, the film was stored in the dryer until it was needed. Finally, the hydrogel was immersed in ZnSO<sub>4</sub> aqueous solution for 2 h and the stable Zn-PVA hydrogel was obtained by ion exchange and additional cross-linking reaction through Zn<sup>2+</sup> coordination.

## 2.4. Structural Characterizations

The morphology and composition of the above materials were characterized by X-ray diffractometer (XRD, Bruker D8 Advance, Karlsruhe, Germany) and scanning electron microscopy (SEM, Tescan MIRA3 LMH, Brno, Czech Republic). The tensile properties were measured at room temperature at a deformation rate of 50 mm min<sup>-1</sup> on universal material testing machines (AG-X plus, Shimadzu Corporation, Shimane, Japan). The N<sub>2</sub> adsorption-desorption isotherms were tested by ASAP 2020 (Micrometrics, Shanghai, China) at 77 K.

## 2.5. Electrochemical Characterizations

VCN-n, acetylene black, and polyvinylidene fluoride (PVDF) were dispersed in NMP (1-Methyl-2-pyrrolidinone) at a ratio of 8:1:1. The slurry was consequently coated on carbon paper (1.0–2.0 cm<sup>2</sup>) and dried as the cathode to dry. Then, the FZIB (~6 cm<sup>2</sup>) on a flexible PET substrate was assembled with VCN-n as cathode, Zn powder as an anode, and a hydrogel electrolyte layer. Typically, the active material loaded on the electrode was 1.0–3.0 mg cm<sup>-2</sup>. Cyclic voltammetry (CV) and galvanostatic charge-discharge (GCD) measurements were used to evaluate the electrochemical performance on the electrochemical workstation (CHI700E). The cycling stability measurement of the FZIB was carried out on a LAND test system (CT2001A) with a sweeping charge and discharge rate at 0.1 mA cm<sup>2</sup> for 1000 consecutive cycles. The resistance changes of the self-power sensor in a different state were obtained by an electrochemical workstation (CHI 700E).

## 3. Results and Discussion

Figure 1a exhibits the XRD images of the nitridation products synthesized at 900 °C for 2 h in a N<sub>2</sub> atmosphere. The diffraction peaks of all samples were 76.4°, 63.7°, 43.8°, and 37.7°, corresponding to the (222), (220), (200), and (111) facets of the VN phase (JCPDS Card no. 78-1315), respectively [17]. All the samples, VN and VCN-n, displayed similar XRD diffraction patterns. The results show that all the samples belong to VN with cubic structures and all were in the Fm3m space group. The corresponding lattice parameters were 4.14 Å. Figure S1 and Figure 1b shows the SEM micro-structure morphology of the four treatments at 900 °C. It is obvious that both VN samples and VCN with glucose have mesoporous nanoribbons. It is obvious in the picture that VCN-5 nanoribbons not only have various sizes of pores, but also have pore sizes about 50 nm. VCN-1 and VCN-3

samples also have similar microstructure. It is not difficult to see that the change of pore size is related to the amount of glucose. With the increase of glucose (VCN-5), the pore diameter becomes more uniform, which is beneficial to the faster movement of ions in electrolytes in electrochemical work, so that the active materials can easily obtain high electrochemical performance. Figure 1b,c gives the typical SEM and TEM image of VCN-5. The TEM image of the corresponding SAED pattern (Figure 1d) shows that the mesoporous nanoribbons are composed of polycrystalline VCN structures with three kinds of crystal planes: (200), (111), and (222). This is consistent with the crystal structure parameters analyzed by XRD.

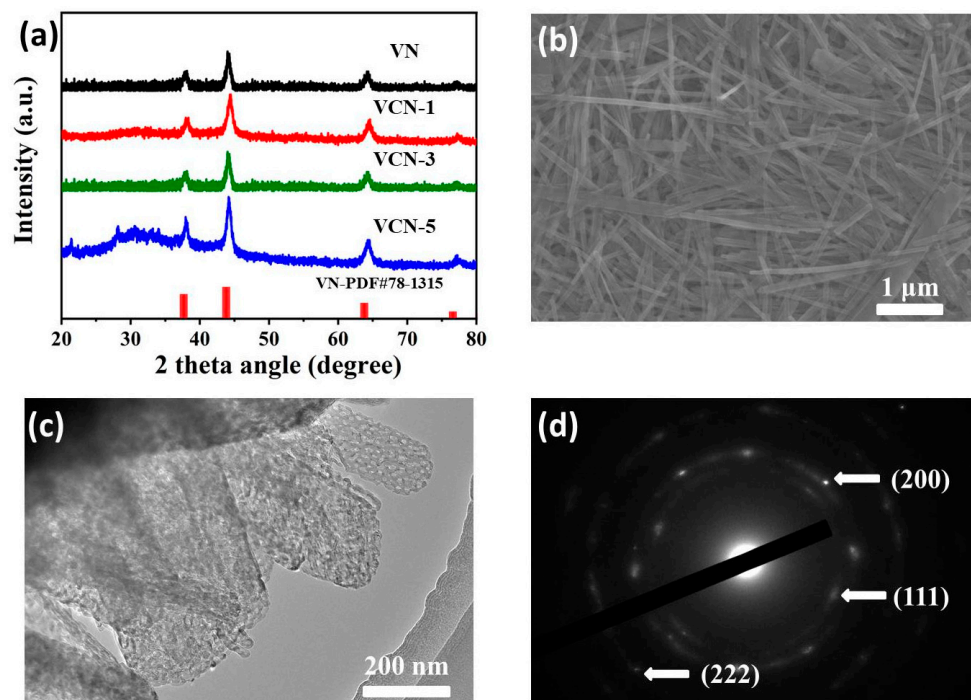


**Figure 1.** (a) Typical XRD image of samples VCN-*n* (*n* = 1, 3, and 5). (b) SEM image of sample VCN-5 and (c) TEM image of sample VCN-5. (d) Corresponding SAED patterns.

As can be seen from Figure 2, all samples had porous structural properties. Their SSA (Specific Surface Area) figures were calculated to be 39.3, 41.1, 45.5, and 54.4 m<sup>2</sup> g<sup>-1</sup> for VN, VCN-1, VCN-3, and VCN-5, respectively, by BET software. Their total pore volumes were 0.221, 0.230, 0.239, and 0.266 cm<sup>3</sup> g<sup>-1</sup> for VN, VCN-1, VCN-3, and VCN-5, respectively. VCN-5 has a higher specific surface area of 54.4 m<sup>2</sup> g<sup>-1</sup>, with total pore volumes of 0.266 cm<sup>3</sup> g<sup>-1</sup>, which further indicates the mesoporous structure. There is no doubt that the mesoporous structure can increase the migration rate of ions on the surface of electrode materials, which is beneficial to the faster movement of ions in electrolytes in electrochemical work. High specific surface area and a mesoporous structure contribute to the improvement of electrochemical performance of supercapacitors. The above results are also consistent with the results of micro-structure images. From this point of view, because of its high specific surface area and better distributed pore structure, VCN-5 has great potential to realize high electrochemical performance in energy storage devices.

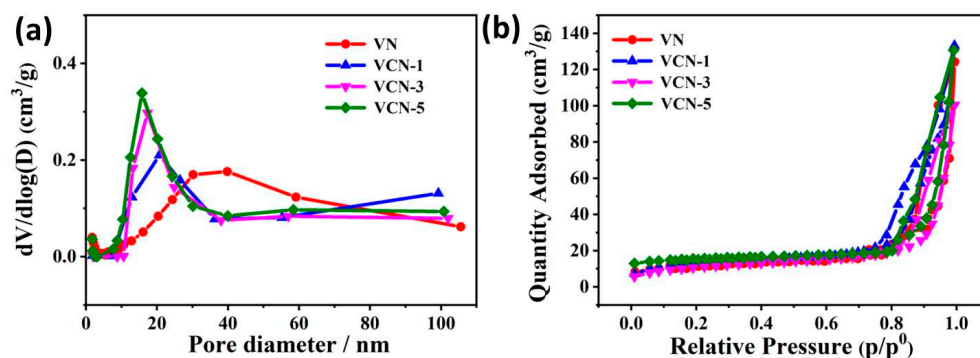


**Figure 2.** The samples of VCN-*n* (*n* = 1, 3, and 5). (a)  $\text{N}_2$  adsorption-desorption isotherms curve at 77 K. (b) Pore volume curve at different relative pressure.

To further evaluate the electrochemical properties of the as-synthesized samples, the whole flexible battery on a flexible PET substrate was assembled with an active material as cathode, Zn powder as an anode, and PVA as electrolyte, as shown in Figure 3a. The CV curves were tested in Figure 3b–e. Authentication of typical CV curves of the VN, VCN-1, VCN-3, and VCN-5 samples was conducted for the first four cycles at a scan rate of  $0.3 \text{ mV s}^{-1}$ . Two oxidation peaks and two reduction peaks on the CV curve at a scanning rate of  $0.3 \text{ mV s}^{-1}$  imply that the intercalation and deintercalation of zinc ions is a multistep process. As the number of cycles increases, the shape and position of the curves tended to be gradually stable. The formation of the two redox peaks is related to the change in the oxidation state of vanadium [18,19]. The CV curves of VN, VCN-1, VCN-3, and VCN-5 are similar; two types of double layer and pseudo capacitor are displayed. After the first four cycles, the CV curves overlap well, indicating that the material is highly reversible. Calculated from the CV curve, their specific capacitances were  $175.2$ ,  $201.8$ ,  $227.1$ , and  $318.2 \text{ mAh g}^{-1}$  at  $100 \text{ mA g}^{-1}$  for samples VN, VCN-1, VCN-3, and VCN-5, respectively. More specifically, VCN-5 has a steady wide electrochemical working voltage of  $0.9$ – $1.9 \text{ V}$ , which exhibits that the shape has not changed much at different cycles. It is further verified that the electrochemical performance of VCN-5 electrode is the best for all samples. The measured capacitance retention of VCN-5 from  $100 \text{ mA g}^{-1}$  to  $1500 \text{ mA g}^{-1}$  (Figure 3e) indicates that the VCN-5 electrode holds a satisfying rate capability. The above test results show that as an active material for energy storage equipment, VCN-5 has higher specific capacity and rate performance than VN, which may be due to the introduction of C element with high electrical conductivity. Therefore, VCN-5 is an ideal cathode material for a zinc-ion battery. In addition, we successfully assembled a ZIB by designing a cross-finger positive and negative electrode energy storage device and using VCN-5 as the active cathode material.

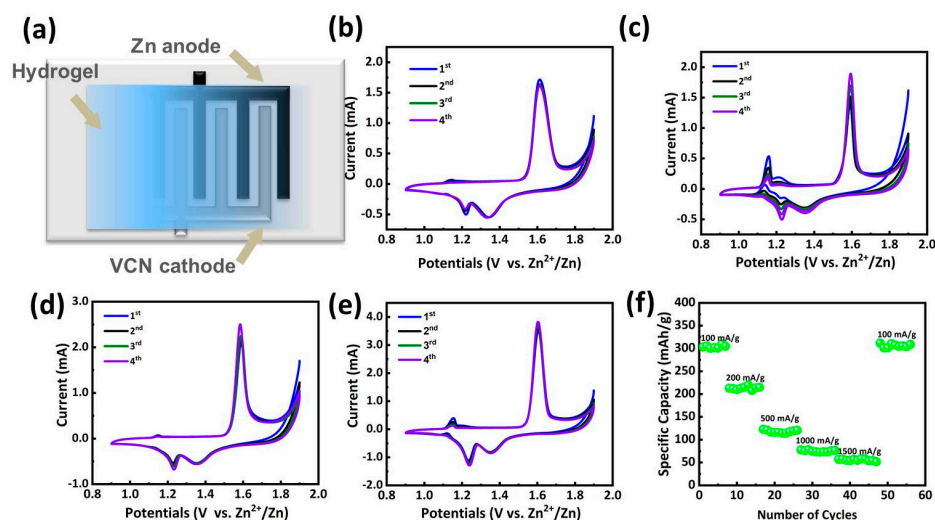


**Figure 3.** (a) Schematic illustration of typical interdigital configured of FZIB. CV curves of VN (b), VCN-1 (c), VCN-3 (d), and VCN-5 (e) for the first four cycles. (f) Rate capability of VCN-5.

Therefore, the whole FZIB ( $\sim 6 \text{ cm}^2$ ) on flexible PET substrate was assembled with VCN-5 as cathode, Zn powder as an anode, and a hydrogel electrolyte layer. Figure 4a shows a typical forked finger shape flexible battery combined on a flexible PET substrate, which successfully powers an electronic clock normally. As shown in Figure S2a, the flexible battery after 1 h, the electronic clock still worked. Using an electronic measuring instrument (Figure S2b) to measure the thickness of the battery, the number was only 0.14 mm, especially thin in thickness. The flexibility test of the miniature battery is shown in Figure S2c. The battery can still work normally after being used at  $180^\circ$ . Based on the above characteristics, this flexible battery provides a broad prospect for a flexible energy storage device, such as electronic skin or wearable electronics.

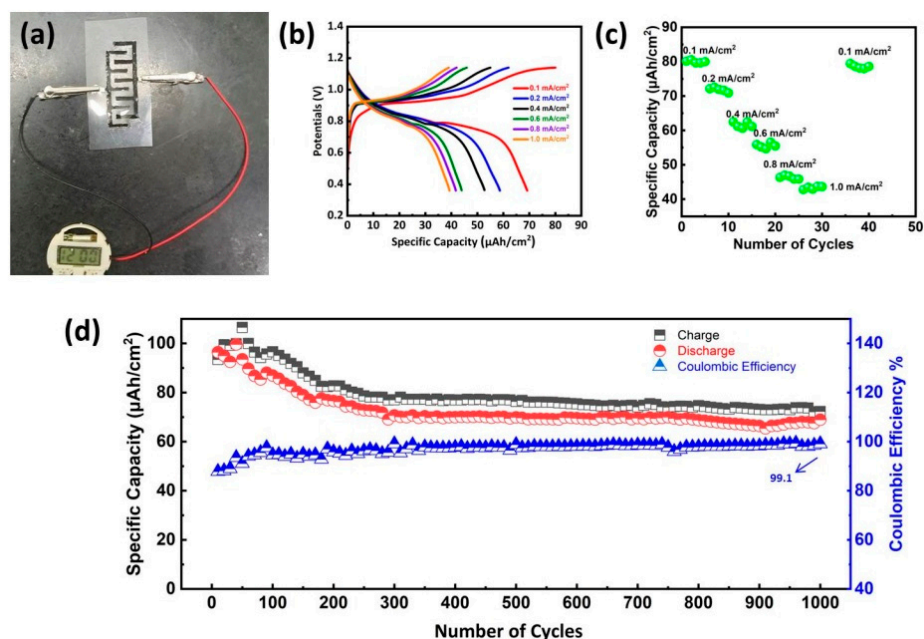


**Figure 4.** The electrochemical performances of FZIB. (a) Typical interdigital configured flexible battery fabricated on a flexible PET substrate, successfully powering a digital clock normally. (b) CV curves with the current density increasing from  $0.1 \text{ mA cm}^{-2}$  to  $1.0 \text{ mA cm}^{-2}$ . (c) The specific capacity with the current density increasing from  $0.1 \text{ mA cm}^{-2}$  to  $1.0 \text{ mA cm}^{-2}$  of FZIB. (d) Cyclic stability and Coulomb efficiency of FZIB. The data was recorded every 10 cycles.

As the current density rises  $0.1 \text{ mA cm}^{-2}$  to  $1.0 \text{ mA cm}^{-2}$ , the specific capacity decreases from  $81$  to  $43 \text{ } \mu\text{Ah cm}^{-2}$  (Figure 4b), suggesting the excellent rate capability of FZIB. In Figure 4c, the GCD curves further confirm the specific capacity with the current density increasing from  $0.1 \text{ mA cm}^{-2}$  to  $1.0 \text{ mA cm}^{-2}$  of FZIB. The results show that FZIB still maintains a good rate capability at different current density. It can be seen from Figure S3 that VCN shows a straight line approximately perpendicular to the abscissa in the low frequency region of the EIS curve before and after cycling, which indicates that the electrode has a fast ion transport speed. After fitting according to the equivalent circuit diagram, the charge transfer resistance ( $R_{ct}$ ) obtained through the semicircle in the high frequency region was  $28.3 \text{ } \Omega$  and  $64.7 \text{ } \Omega$ , respectively. The small resistance before and after the cycle shows excellent electron transport performance, high conductivity, and fast ion transport to ensure that ions can reach the active site faster and in greater quantity, as well as improve the utilization of the active site, which is the advantage of the porous structure of VCN. Due to the high conductivity of the active material and the collector, on the other hand, the transport path of electrolytic ions in the specially designed cross-finger electrode is shortened, which makes the transport between particles more efficient. These reasons make FZIB have good rate performance, in addition to the cycling stability and coulomb efficiencies of the FZIB in Figure 4d. It is not difficult to see that FZIB not only maintains 77% at  $0.6 \text{ mA cm}^{-2}$  current density, but also maintains a very high coulomb efficiency in electrochemical work.

#### 4. Conclusions

In the paper, we have successfully prepared VCN nanobelts, which display mesoporous structure with a relatively large specific surface area ( $54.4 \text{ m}^2 \text{ g}^{-1}$ ) and a total pore volume of  $0.266 \text{ cm}^3 \text{ g}^{-1}$ . As an ideal cathode material for the battery, VCN nanobelts exhibit a specific capacitance of  $318.2 \text{ mAh g}^{-1}$  at  $100 \text{ mA g}^{-1}$ . Additionally, the prepared FZIB with VCN-5 not only exhibited high specific capacitance ( $81 \text{ } \mu\text{Ah cm}^{-2}$ ), excellent rate capability, and long cyclic durability (77% after 1000 cycles at  $0.6 \text{ mA cm}^{-2}$ ) but also had characteristics of flexibility. This work provides a simple and efficient scheme for the design and manufacture of FZIB and other micro energy storage devices, and is of practical significance to solve the energy supply problems of miniaturized, portable, and flexible wearable electronic devices. This FZIB is important for the development of applications such as miniaturized, flexible, portable, and wearable electronics, while reducing the difficulty in thermal management.

**Supplementary Materials:** The following supporting information can be downloaded at: <https://www.mdpi.com/article/10.3390/en15134932/s1>, Figure S1: Typical SEM of sample (a) VN, (b) VCN-1 and (c) VCN-3. Figure S2. (a) the flexible battery after 1 h can still power a digital clock normally. (b) Thickness of the FZIB, the number shows that only 0.14 mm. (c) The flexibility test of the FZIB. Figure S3. EIS curve before and after cycling, with the equivalent circuit model in the lower right corner. Figure S4. Representative EDX spectrum of sample (a) VCN-1 and (b) VCN-3. Table S1. Comparison of Electrochemical performance between VCN electrode and other previously reported Vanadium-based Electrodes. (References [1,20–27] are cited in the supplementary materials).

**Author Contributions:** Conceptualization, Z.Z.; methodology, Z.Z.; software, T.Z. and H.Z.; validation, Z.Z. and T.Z.; formal analysis, T.Z. and H.Z.; investigation, Z.Z. and T.Z.; resources, Z.Z. and T.Z.; data curation, Z.Z. and T.Z.; writing—original draft preparation, Z.Z.; writing—review and editing, Z.Z.; visualization, Z.Z.; supervision, D.C.; project administration, Z.Z. and D.C. All authors have read and agreed to the published version of the manuscript.

**Funding:** This research received no external funding.

**Institutional Review Board Statement:** Not applicable.

**Informed Consent Statement:** Not applicable.

**Data Availability Statement:** The data that support the findings of this study are available from the corresponding author, [Z.Z.], upon reasonable request.

**Conflicts of Interest:** The authors declare no conflict of interest.

## References

1. Su, Q.; Rong, Y.; Chen, H.; Wu, J.; Yang, Z.; Deng, L.; Fu, Z. Carbon-Doped Vanadium Nitride Used as a Cathode of High-Performance Aqueous Zinc Ion Batteries. *Ind. Eng. Chem. Res.* **2021**, *60*, 12155–12165. [[CrossRef](#)]
2. Ray, A.; Saruhan, B. Application of Ionic Liquids for Batteries and Supercapacitors. *Materials* **2021**, *14*, 2942. [[CrossRef](#)]
3. Jiang, H.; Zhang, Y.; Pan, Z.; Xu, L.; Zheng, J.; Gao, Z.; Hu, T.; Meng, C.; Wang, J.  $\text{NH}_4\text{V}_3\text{O}_8 \cdot 0.5\text{H}_2\text{O}$  nanobelts with intercalated water molecules as a high performance zinc ion battery cathode. *Mater. Chem. Front.* **2020**, *4*, 1434–1443. [[CrossRef](#)]
4. Armand, M.; Tarascon, J.M. Building better batteries. *Nature* **2008**, *451*, 652–657. [[CrossRef](#)]
5. Tarascon, J.M.; Armand, M. Issues and challenges facing rechargeable lithium batteries. *Nature* **2001**, *414*, 359–367. [[CrossRef](#)]
6. Ni, J.; Fu, S.; Wu, C.; Maier, J.; Yu, Y.; Li, L. Self-Supported Nanotube Arrays of Sulfur-Doped  $\text{TiO}_2$  Enabling Ultrastable and Robust Sodium Storage. *Adv. Mater.* **2016**, *28*, 2259–2265. [[CrossRef](#)]
7. Pramudita, J.C.; Sehwat, D.; Goonetilleke, D.; Sharma, N. An Initial Review of the Status of Electrode Materials for Potassium-Ion Batteries. *Adv. Energy Mater.* **2017**, *7*, 1602911. [[CrossRef](#)]
8. Chen, S.; Wu, C.; Shen, L.; Zhu, C.; Huang, Y.; Xi, K.; Maier, J.; Yu, Y. Challenges and Perspectives for NASICON-Type Electrode Materials for Advanced Sodium-Ion Batteries. *Adv. Mater.* **2017**, *29*, 1700431. [[CrossRef](#)]
9. Xu, C.; Li, B.; Du, H.; Kang, F. Energetic zinc ion chemistry: The rechargeable zinc ion battery. *Angew Chem. Int. Ed. Engl.* **2012**, *51*, 933–935. [[CrossRef](#)]
10. Parker, J.F.; Chervin, C.N.; Pala, I.R.; Machler, M.; Burz, M.F.; Long, J.W.; Rolison, D.R. Rechargeable nickel-3D zinc batteries: An energy-dense, safer alternative to lithium-ion. *Science* **2017**, *356*, 415–418. [[CrossRef](#)]
11. Gu, P.; Zheng, M.; Zhao, Q.; Xiao, X.; Xue, H.; Pang, H. Rechargeable zinc-air batteries: A promising way to green energy. *J. Mater. Chem. A* **2017**, *5*, 7651–7666. [[CrossRef](#)]
12. Li, Y.; Dai, H. Recent advances in zinc-air batteries. *Chem. Soc. Rev.* **2014**, *43*, 5257–5275. [[CrossRef](#)] [[PubMed](#)]
13. Hao, J.; Mou, J.; Zhang, J.; Dong, L.; Liu, W.; Xu, C.; Kang, F. Electrochemically induced spinel-layered phase transition of  $\text{Mn}_3\text{O}_4$  in high performance neutral aqueous rechargeable zinc battery. *Electrochim. Acta.* **2018**, *259*, 170–178. [[CrossRef](#)]
14. Wang, X.; Wang, F.; Wang, L.; Li, M.; Wang, Y.; Chen, B.; Zhu, Y.; Fu, L.; Zha, L.; Zhang, L.; et al. An Aqueous Rechargeable  $\text{Zn}/\text{Co}_3\text{O}_4$  Battery with High Energy Density and Good Cycling Behavior. *Adv. Mater.* **2016**, *28*, 4904–4911. [[CrossRef](#)]
15. Senguttuvan, P.; Han, S.D.; Kim, S.; Lipson, A.L.; Tepavcevic, S.; Fister, T.T.; Bloom, I.D.; Burrell, A.K.; Johnson, C.S. A High Power Rechargeable Nonaqueous Multivalent  $\text{Zn}/\text{V}_2\text{O}_5$  Battery. *Adv. Energy Mater.* **2016**, *6*, 1600826. [[CrossRef](#)]
16. Liu, Z.; Cui, T.; Pulletikurthi, G.; Lahiri, A.; Carstens, T.; Olschewski, M.; Endres, F. Dendrite-Free Nanocrystalline Zinc Electrodeposition from an Ionic Liquid Containing Nickel Triflate for Rechargeable Zn-Based Batteries. *Angew. Chem. Int. Ed. Engl.* **2016**, *55*, 2889–2893. [[CrossRef](#)]
17. Zhou, Z.; Liang, Z.; Shao, G.; Liu, Q.; Chen, D.; Yang, W. Enhanced Capacitive Performance of Mesoporous Vanadium Nitride Nanobelts. *J. Electrochem. Soc.* **2021**, *168*, 070529. [[CrossRef](#)]
18. Choi, D.; Kumta, P.N. Chemically Synthesized Nanostructured VN for Pseudocapacitor Application. *Electrochem. Solid-State Lett.* **2005**, *8*, A418. [[CrossRef](#)]
19. Choi, D.; Blomgren, G.E.; Kumta, P.N. Fast and Reversible Surface Redox Reaction in Nanocrystalline Vanadium Nitride Supercapacitors. *Adv. Mater.* **2006**, *18*, 1178–1182. [[CrossRef](#)]
20. Guo, J.; Ming, J.; Lei, Y.; Zhang, W.; Xia, C.; Cui, Y.; Alshareef, H.N. Artificial Solid Electrolyte Interphase for Suppressing Surface Reactions and Cathode Dissolution in Aqueous Zinc Ion Batteries. *ACS Energy Lett.* **2019**, *4*, 2776–2781. [[CrossRef](#)]
21. Wang, X.; Xi, B.; Ma, X.; Feng, Z.; Jia, Y.; Feng, J.; Qian, Y.; Xiong, S. Boosting Zinc-Ion Storage Capability by Effectively Suppressing Vanadium Dissolution Based on Robust Layered Barium Vanadate. *Nano Lett.* **2020**, *20*, 2899–2906. [[CrossRef](#)] [[PubMed](#)]
22. Tang, W.; Lan, B.; Tang, C.; An, Q.; Chen, L.; Zhang, W.; Zuo, C.; Dong, S.; Luo, P. Urchin-like Spinel  $\text{MgV}_2\text{O}_4$  as a Cathode Material for Aqueous Zinc-Ion Batteries. *ACS Sustain. Chem. Eng.* **2020**, *8*, 3681–3688. [[CrossRef](#)]
23. Bin, D.; Wang, Y.; Tamirat, A.G.; Zhu, P.; Yang, B.; Wang, J.; Huang, J.; Xia, Y. Stable High-Voltage Aqueous Zinc Battery Based on Carbon-Coated  $\text{NaVPO}_4\text{F}$  Cathode. *ACS Sustain. Chem. Eng.* **2021**, *9*, 3223–3231. [[CrossRef](#)]
24. Shan, X.; Kim, S.; Abeykoon, A.M.M.; Kwon, G.; Olds, D.; Teng, X. Potentiodynamics of the Zinc and Proton Storage in Disordered Sodium Vanadate for Aqueous Zn-Ion Batteries. *ACS Appl. Mater. Interfaces* **2020**, *12*, 54627–54636. [[CrossRef](#)] [[PubMed](#)]
25. Li, Z.; Wu, B.; Yan, M.; He, L.; Xu, L.; Zhang, G.; Xiong, T.; Luo, W.; Mai, L. Novel Charging-Optimized Cathode for a Fast and High-Capacity Zinc-Ion Battery. *ACS Appl. Mater. Interfaces* **2020**, *12*, 10420–10427. [[CrossRef](#)]
26. Wang, M.; Zhang, J.; Zhang, L.; Li, J.; Wang, W.; Yang, Z.; Zhang, L.; Wang, Y.; Chen, J.; Huang, Y.; et al. Graphene-like Vanadium Oxygen Hydrate (VOH) Nanosheets Intercalated and Exfoliated by Polyaniline (PANI) for Aqueous Zinc-Ion Batteries (ZIBs). *ACS Appl. Mater. Interfaces* **2020**, *12*, 31564–31574. [[CrossRef](#)]
27. Nagaraj, R.; Pakhira, S.; Aruchamy, K.; Yadav, P.; Mondal, D.; Dharmalingam, K.; Sanna Kotrappanavar, N.; Ghosh, D. Catalyzing the Intercalation Storage Capacity of Aqueous Zinc-Ion Battery Constructed with Zn(II) Preinserted Organo-Vanadyl Hybrid Cathode. *ACS Appl. Energy Mater.* **2020**, *3*, 3425–3434. [[CrossRef](#)]